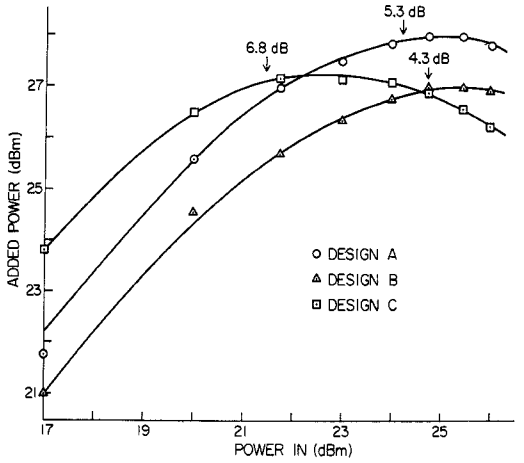

Fig. 9. Experimentally measured added power as a function of input power for the three designs of Fig. 5.

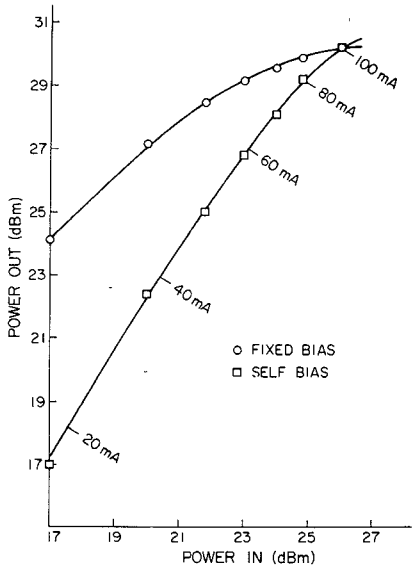

Fig. 10. Experimentally measured output power as a function of input power for the amplifier of design A, under both fixed-bias operation and self-bias operation. For fixed-bias operation, V_{CC} = 20 V; I_C = 100 mA. For self-bias operation, V_{CC} = 20 V, and I_C is as indicated in the figure.

is approximately 1 dB less than the measured small-signal power gain. The data of Fig. 8 are replotted in Fig. 9 to show that the predicted values of large-signal power gain did indeed occur near the point of maximum added power.

All of the preceding data are for fixed-bias operation (class A operation). In many cases, however, a microwave transistor power amplifier is operated under self-bias conditions (class C operation). The question arises whether the design procedure described here also applies to such self-bias operation. To investigate, the test amplifier was modified for self-bias operation by grounding the base bias lead. The results of this test are shown in Fig. 10. This figure shows that the performance of the self-biased amplifier became identical to the performance of the fixed-bias amplifier at the exact point where the self-bias operating point became identical to the fixed-bias operating point. Hence this design approach appears to be valid for both fixed-bias and self-bias amplifiers.

Conclusion

A method of large-signal device characterization and power amplifier design has been described and shown to be valid for a 1-W silicon BJT operating at 1.3 GHz. This approach not only allows the designer to predict the load and source terminations required for optimum added-power circuit efficiency, but also graphically shows how efficiency and power gain change with different load terminations. The method is felt to be generally applicable at frequencies sufficiently high such that significan clipping does not occur at the output of the device. While the precise lower limit of this frequency range is not presently known, experimental results indicate that it should be valid for those frequencies where the added-power circuit efficiency is 50 percent or less.

References

[1] A. Presser and E. Belohoubek, "1–2 GHz high-power linear amplifier," *RCA Rev.*, vol. 33, pp. 737–751, Dec. 1972.
[2] O. Pitzalis, Jr., and R. A. Gilson, "Broad-band microwave class-C transistor amplifiers," *IEEE Trans. Microwave Theory Tech.*, vol. MTT-21, pp. 660–668, Nov. 1973.
[3] J. M. Cusack, S. M. Perlow, and B. S. Perlman, "Automatic load contour mapping for microwave power transistors," *IEEE Trans. Microwave Theory Tech.*, vol. MTT-22, pp. 1146–1152, Dec. 1974.
[4] W. H. Leighton, R. J. Chaffin, and J. G. Webb, "RF amplifier design with large-signal *s*-parameters," *IEEE Trans. Microwave Theory Tech.*, vol. MTT-21, pp. 809–814, Dec. 1973.
[5] L. S. Houselander, H. Y. Chow, and R. Spence, "Transistor characterization by effective large-signal two-port parameters," *IEEE J. Solid-State Circuits*, vol. SC-5, pp. 77–79, April 1970.
[6] R. Spence, *Linear Active Networks*. New York: Wiley-Interscience, 1970.
[7] K. L. Kotzebue, "The use of large-signal *y*-parameters in high frequency transistor circuit design," *Proceedings Ninth Annual Asilomar Conference on Circuits, Systems, and Computers*, Nov. 1975.
[8] J. G. Linvill and L. G. Schimpf, "The design of tetrode transistor amplifiers," *Bell Syst. Tech. J.*, vol. 35, pp. 813–840, 1956.
[9] J. G. Linvill and J. F. Gibbons, *Transistors and Active Circuits*. New York: McGraw-Hill, 1961.

Passive Millimeter-Wave IC Components Made of Inverted Strip Dielectric Waveguides

R. RUDOKAS AND T. ITOH, SENIOR MEMBER, IEEE

***Abstract*—New directional couplers and ring resonators for millimeter-wave IC's were fabricated from the inverted strip (IS) dielectric waveguide. They were tested in the 75–80-GHz range, and the agreement between the theoretical and experimental results was found to be good.**

I. Introduction

Inherent limitations in conventional metal waveguides at millimeter wavelengths have spurred research into alternate guiding structures [1]–[4]. In particular, the inverted strip (IS) dielectric waveguide [5] shows promise from the standpoint of low loss, ease of fabrication, and convenient size. Comparison

Manuscript received March 17, 1976; revised July 21, 1976. This work was supported in part by the Joint Services Electronics Program DAAB07-72-G0113, and in part by the U.S. Army Research Office under Grant DAHC04-74-G0113.

R. Rudokas is with the Coordinated Science Laboratory and the Department of Electrical Engineering, University of Illinois at Urbana-Champaign, Urbana, IL 61801.

T. Itoh was with the Coordinated Science Laboratory and the Department of Electrical Engineering, University of Illinois at Urbana-Champaign, Urbana, IL 61801. He is now with the Stanford Research Institute, Menlo Park, CA 94025.

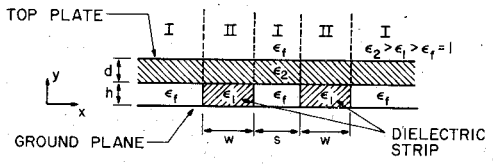

Fig. 1. Cross section of coupled IS guide.

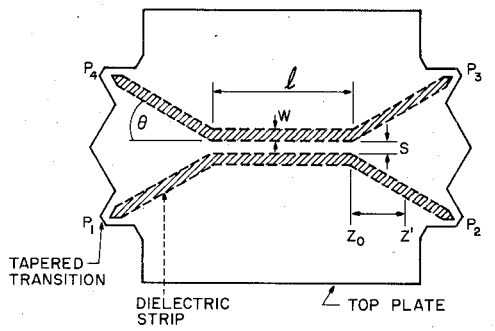

Fig. 2. Top view of distributed directional coupler.

between this and other millimeter waveguides is included in [5]. Also included there is a detailed analysis of the IS waveguide.

This short paper discusses the distributed directional coupler, the beam-splitter-type directional coupler, and the ring resonator fabricated with the IS waveguide. Both numerical and experimental results are presented and compared.

The basic IS guide structure is as shown in Fig. 1. A major portion of the energy propagates in the top plate (typically fused quartz) which has the highest dielectric constant ε_2 of the three media. A lens effect, created by the dielectric strips (typically Teflon) of dielectric constant ε_1 beneath the top plate, localizes this energy in the region directly above the strips. Conductor loss for this structure is low since there is a separation (h) between the ground plane and the propagating energy, yet the ground plane is available as a heat sink and dc bias return for solid-state devices mounted in the IS guide.

II. Distributed Directional Coupler

The distributed coupler consists of a section of a coupled IS guide of length l and separation s with four connecting guides as shown in Fig. 2. If we assume that the coupling due to the connecting guides is negligible, then the length L needed to completely transfer energy incident at port 1 to port 3 is given by [6]

$$L = \frac{\pi}{k_{ze} - k_{z0}} \tag{1}$$

where k_{ze} and k_{z0} are functions of the separation s of the coupled guide. Given some length of coupled guide l, the ratio of the power at ports 2 and 3 is

$$\frac{P_3}{P_2} = \tan^2\left(\frac{\pi l}{2L}\right). \tag{2}$$

In the preceding analysis, the coupling between the connecting guides was ignored. This coupling may not be trivial and must be included in the analysis of the coupler. Equation (2) can then be modified to include this additional effect in the following manner:

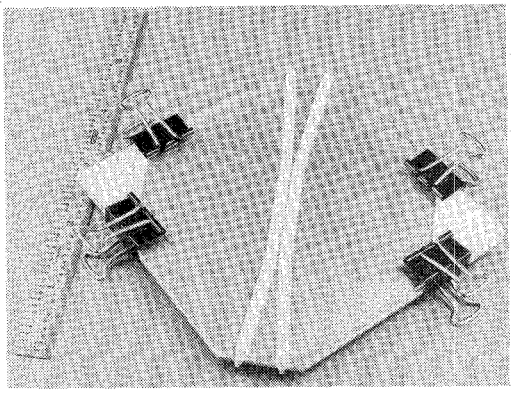

Fig. 3. Distributed directional coupler.

$$\frac{P_3}{P_2} = \tan^2\left(\frac{\pi l}{2L}\right) \tag{3}$$

where the effective length is

$$l = l + \frac{\Delta\phi}{\pi} L \tag{4}$$

$$\Delta\phi = 2\int_{z0}^{z'} [k_{ze}(z) - k_{z0}(z)]\, dz. \tag{5}$$

In (5), the integration is carried out along the axial (z) direction of the directional coupler. z_0 corresponds to the junction between the coupled guide and the connecting arm, while z' is chosen to be some value of z beyond which the coupling between the arms is negligible, and k_{ze} is practically identical to k_{z0}. The factor of 2 occurs because of the symmetry of the coupler; otherwise, a different integration would have to be made for the other side of the coupler.

When the coupler is designed, the relation between L and s may be used to estimate the required length l of the coupler. This coupler is expected to be slightly different in performance from theoretical predictions, since we have ignored the coupling between connecting guides as described in (3)–(5). However, by slightly adjusting the separation s, the desired coupling performance may still be obtained.

A photograph of a typical distributed directional coupler is shown in Fig. 3. Teflon and fused quartz are used for the dielectric strip and the top plate, respectively. Notice that the major portion of millimeter-wave energy propagates in the quartz plate, not in the Teflon strip.

III. Beam-Splitter-Type Directional Coupler

The coupler shown in Fig. 4(a) is based on the principle of the optical beam splitter. The coupler consists of two perpendicular intersection guides, in which a gap s, oriented at 45° to each guide, is made in the dielectric strips. The effective dielectric constant of this gap portion is ε_{e1} corresponding to the top plate floating above the ground plane, while in the regions where the dielectric strips are present, it is ε_{e2}. Therefore, the coupling structure can be replaced with the sandwiched structure shown in Fig. 4(b).

As a simple first-order approximation, the phase front of the dominant mode in the IS guide is similar to that of a plane wave. Using Fig. 4(b) we can easily calculate a reflection coefficient

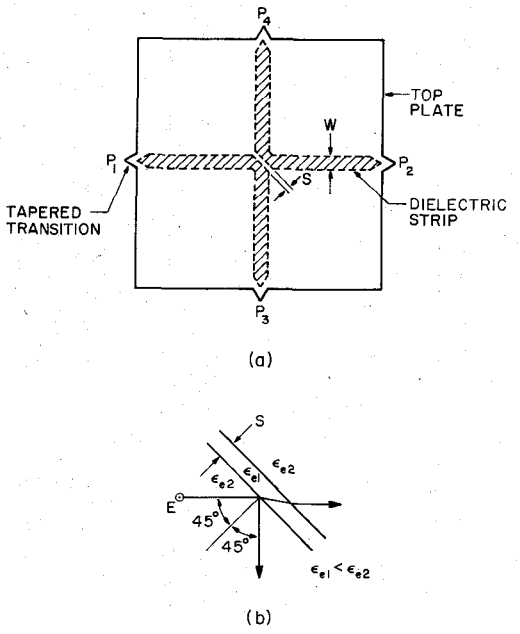

Fig. 4. (a) Top view of beam-splitter-type directional coupler. (b) Equivalent geometry.

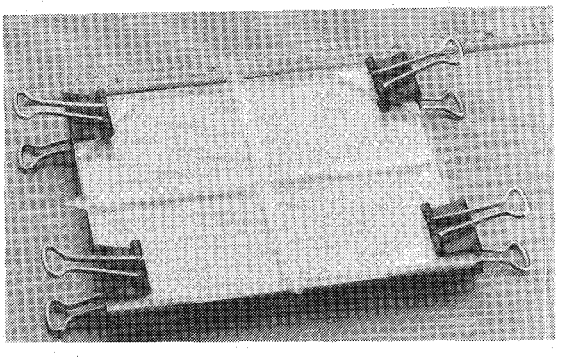

Fig. 5. Beam-splitter-type coupler.

for the E^y modes ρ due to the discontinuity in the dielectric constants at the gap.

$$|\rho|^2 = \frac{\left(\alpha - \frac{1}{\alpha}\right)^2 \tan^2\left(k_0 sp\sqrt{\frac{\varepsilon_{e1}}{2}}\right)}{4 + \left(\alpha + \frac{1}{\alpha}\right)^2 \tan^2\left(k_0 sp\sqrt{\frac{\varepsilon_{e1}}{2}}\right)} \tag{6}$$

where

$$\alpha = q/p \qquad p = \sqrt{2 - \left(\frac{\varepsilon_{e2}}{\varepsilon_{e1}}\right)} \qquad q = \sqrt{\frac{\varepsilon_{e2}}{\varepsilon_{e1}}} \tag{7}$$

and k_0 is the free-space wave number.

Since energy incident at port 1 is reflected into port 3, the coupling is

$$\frac{P_3}{P_1} = |\rho|^2. \tag{8}$$

In the design of the beam-splitter-type coupler, s is the only parameter to be adjusted in order to obtain the desired coupling, once the IS guide structures (w, h, d, ε_1, and ε_2) are fixed. A typical beam-splitter-type coupler is shown in Fig. 5 where a Teflon strip and a fused quartz top plate are used in fabrication.

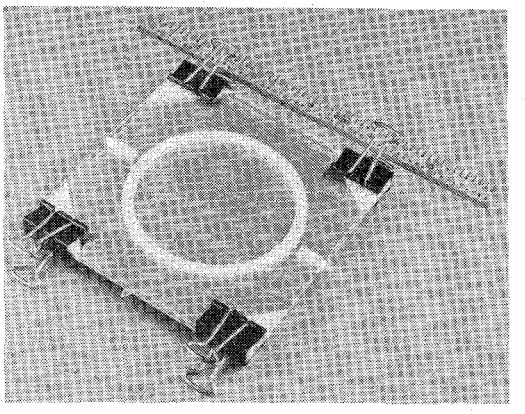

Fig. 6. Ring resonator.

IV. Ring Resonator

A photo of an IS guide ring resonator is shown in Fig. 6. Once again a fused quartz plate is used as the top plate on the Teflon ring. Resonance conditions for the resonator are

$$n\lambda_g = 2\pi\bar{r}, \qquad n = 1,2,3,\cdots \tag{9}$$

where λ_g is the wavelength in the ring and $\bar{r}$ is the effective radius of the ring. If the width of the ring is small compared to the radius, $\bar{r} \approx \sqrt{ab}$, where a and b are the outer and inner radii.

When the radius of curvature is large, we can approximate λ_g by the guide wavelength in a straight section of an IS guide. Using these approximations, the resonant frequencies are calculated.

V. Results and Discussions

The experiments were conducted over the range of 75–80 GHz using a mechanically tuned IMPATT diode oscillator. Power measurements were made using tuned diode detectors in RG 99/U waveguide coupled to the IS waveguide through a tapered quartz tip. The edge of the quartz plate was ground to produce the tip. Teflon dielectric strips were either cut or machined from Teflon sheet and round stock. A sufficient amount of mechanical pressure was applied to eliminate the air gap between the layers.

Fig. 7 shows the measured and calculated characteristics of a distributed directional coupler fabricated with Teflon and quartz. The power ratios P_3/P_2 were computed using both the actual and effective lengths, l and $\bar{l}$. When the coupling between the connecting guides is taken into account by the use of (4), the computed and measured ratios differ by about 1.5 dB. The most likely source of this discrepancy is the radiation effect at the junction between the connecting guides and the coupler itself. The measured directivity is not indicative of optimum coupler performance because of an imperfect match between the dielectric and metal waveguide.

The performance of the beam-splitter-type directional coupler is shown in Fig. 8. The insertion-loss curve was obtained by comparison of the total loss from ports 1 to 2 of the coupler with the loss of a straight section of a single IS guide of identical length. The discrepancy between the measured and predicted data on coupling should be due to over-simplified theory in which radiation and scattering phenomena at the junction are totally ignored.

Fig. 9 shows the frequency response curve of the ring resonator. With respect to the computed resonances, the measured even-order resonances are shifted about 0.2 GHz toward the lower

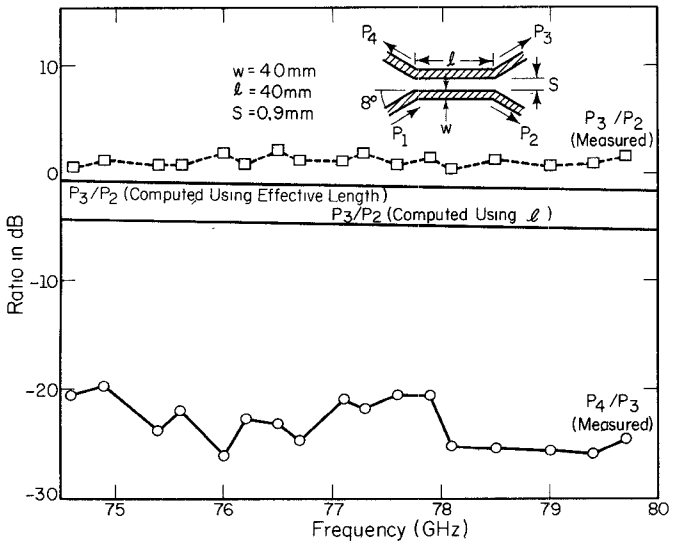

Fig. 7. Computed and measured performance of distributed directional coupler.

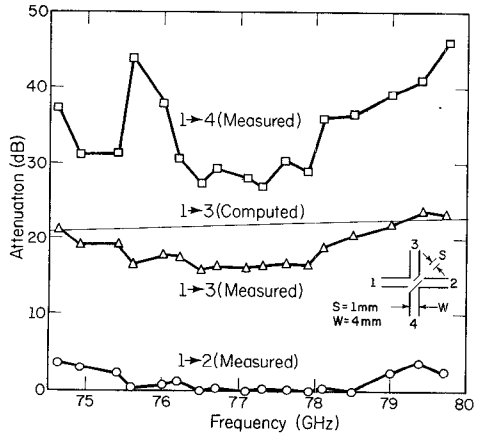

Fig. 8. Computed and measured performance of beam-splitter-type coupler.

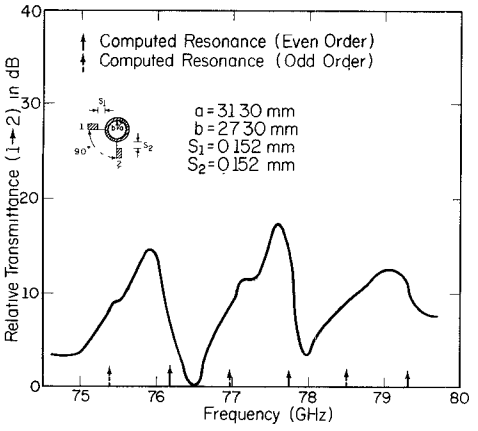

Fig. 9. Transmission characteristics of ring resonator.

frequencies, probably due to the strong coupling effects, while the odd-order resonances remain essentially unshifted. The location of the coupling arm 90° from the excitation arm places it at a null for odd-order resonances. This causes the weak response of the odd-order resonances as seen in the frequency characteristics of the ring resonator. Q of the resonator was found to be too low to be practical in its present form, mainly due to radiation associated with the curve. It is necessary to investigate and reduce the radiation phenomena by choice of material, structural parameters, etc.

VI. Conclusions

Several passive components for the IS millimeter-wave IC's have been described and analyzed. Results for theoretical as well as experimental studies were presented and reasonable agreement was observed. The salient design features for fabrication of these components have also been presented.

References

[1] M. V. Schneider, "Millimeter-wave integrated circuits," *IEEE MTT Symposium*, Boulder, CO, pp. 16–18, June 1973.
[2] P J. Meier, "Two new integrated-circuit media with special advantages at millimeter wavelengths," *IEEE MTT Symposium*, Chicago, IL, May 22–24, 1972.
[3] H. Jacobs and M. M. Crepta, "Electronic phase shifter for millimeter-wave semiconductor dielectric integrated circuits," *IEEE Trans. Microwave Theory Tech.*, vol. MTT-22, no. 4, pp. 411–417, April 1974.
[4] R. M. Knox and P. P. Toulios, "A V-band receiver using image line integrated circuits," *Proc. National Electronics Conf.*, vol. 27, pp. 489–492, Oct. 1974.
[5] T. Itoh, "Inverted strip dielectric waveguide for millimeter-wave integrated circuits," *IEEE Trans. Microwave Theory Tech. (Special Issue on Millimeter Waves, Circuits, Components, and Systems)*, vol. MTT-24, pp. 821–827, Nov. 1976.
[6] K. Kurokawa, *An Introduction to the Theory of Microwave Circuits*. New York: Academic Press, 1969.

Design, Implementation, and Performance Analysis of a Broad-Band V-Band Network Analyzer

L. T. YUAN, G. M. YAMAGUCHI, MEMBER, IEEE, AND J. E. RAUE, MEMBER, IEEE

***Abstract*—A novel V-band network analyzer has been developed for circuit and/or device characterization in the 55–65-GHz frequency range. Swept frequency techniques are utilized to simplify device design and network analysis over a wide range of operating frequencies. The design, fabrication, and performance of the unit is presented along with an error analysis for verification of measurement accuracies.**

Introduction

In recent years network analyzers have been used extensively for circuit and device characterization. They are powerful tools for optimizing circuit or device performance, particularly for broad-band applications where circuit or device parameters have to be known over a wide range of frequencies. However, commercial network analyzers currently available can only be operated up to *Ka*-band frequencies (26.5–40 GHz). For frequencies higher than *Ka* band, circuit and device characterization has to rely on the slotted line techniques by performing fixed-frequency point-by-point measurements. The fixed-frequency point-by-point measurements are not only tedious and time consuming, but also quite often fail to identify resonances between measurement points.

Increasing interest in communications systems operating at V-band frequencies (50–75 GHz) has created the need for the evaluation of circuits and devices at V-band frequencies. It is this demand that has prompted the development of a V-band network analyzer. This unit is capable of operation over a

Manuscript received May 20, 1976; revised July 23, 1976.
The authors are with the TRW Systems Group, Redondo Beach, CA 90278.